Inter- and intratrimer excitations in the multiferroic $Ba_3NbFe_3Si_2O_{14}$

H. D. Zhou,[1,*] Y. Barlas,[1] C. R. Wiebe,[1,2] Y. Qiu,[3,4] J. R. D. Copley,[3] and J. S. Gardner[3,5]
[1]*National High Magnetic Field Laboratory, Florida State University, Tallahassee, Florida 32306-4005, USA*
[2]*Department of Chemistry, University of Winnipeg, Winnipeg, Manitoba, Canada R3B 2E9*
[3]*NIST Center for Neutron Research, Gaithersburg, Maryland 20899-6102, USA*
[4]*Department of Materials Science and Engineering, University of Maryland, College Park, Maryland 20742, USA*
[5]*Indiana University, 2401 Milo B. Sampson Lane, Bloomington, Indiana 47408, USA*
(Received 20 July 2010; revised manuscript received 30 August 2010; published 28 October 2010)

Elastic and inelastic neutron-scattering experiments have been performed on single crystals of the multiferroic $Ba_3NbFe_3Si_2O_{14}$. It is found that the organization of the spin clusters into true long-range ordered states occurs by the following process: (i) by 60 K, there is evidence for short-range ordered triangular Fe clusters of spins, (ii) below 40 K, the clusters begin to form long-range ordered structures as a spin-wave spectrum develops, (iii) at $T_N=26$ K, the sample exhibits coexisting long-range and short-range ordered structures, and (iv) by $T=1.5$ K, a long-range ordered structure with a well-defined spin-wave spectrum develops. The spin-wave excitation can be described by a Heisenberg Hamiltonian within a distorted triangular lattice including both the intratrimer and intertrimer interactions. Physical property measurements showing anomalies near $T=40$ K can now be adequately explained as being due to scattering from low-energy spin fluctuations.

DOI: 10.1103/PhysRevB.82.132408 PACS number(s): 75.47.Lx, 61.05.F−, 75.25.−j

Most geometrically frustrated magnets that have been studied over the last decade consist of a fundamental unit of three spins on the vertices of a triangle. In two dimensions (2D), this has been realized through the edge-shared triangular lattice[1–6] and the corner-shared triangular lattice (kagome lattice).[7–9] Isolated triangular plaquettes are another topology which has remained somewhat elusive due to very few examples existing within the current literature. The compound $La_4Cu_3MoO_{12}$ is a good example of a weakly interacting network of copper spin-1/2 trimers,[10] in which quantum fluctuations play an important role in the nature of the ground state. One central feature of the triangular lattice is its spin chirality. When the interactions among the spins constrained within the triangular plane are antiferromagnetic, the best energetic compromise, in general, is a noncollinear structure with neighboring spins oriented $2\pi/3$ relative to each other. In this local structure the spins can rotate by either $2\pi/3$ or $-2\pi/3$ degrees from unit to unit, which defines the chirality (for clockwise or anticlockwise rotation). The development of a chirality is an important aspect of frustrated magnetic systems, as it implies the emergence of an order parameter which is based on a noncentrosymmetric symmetry. A well-studied example of spin chirality developing in a 2D-frustrated system is the jarosite $KFe_3(OH)_6(SO_4)_2$,[9] in which the definite chiral spin structure emerges before the magnetic ordering involving the vector spins.

$Ba_3NbFe_3Si_2O_{14}$ is another rare geometrically frustrated magnet with isolated Fe^{3+} trimers. It crystallizes in the noncentrosymmetric $P321$ trigonal space group. The Fe^{3+} ions (the only magnetic species) occupy the $3f$ Wyckoff positions and form a network of isolated triangular units within the *ab* plane [Fig. 1(a)]. Recent neutron-scattering experiments have been interpreted with the emergence of a single triangular chirality within the *ab* plane (with a single helicity along the *c* axis) below the antiferromagnetic transition at $T_N=26$ K.[11] How the chirality ordering and spin ordering evolve with temperature in this material has been, unknown, making comparisons with other 2D-frustrated systems challenging. The specific-heat data have shown anomalies at high temperatures which suggest that a short-range ordered spins may be present,[12–14] but this process has never been visualized through probes such as neutron scattering.

In this Brief Report, we present detailed elastic and inelastic neutron-scattering measurements on powder and single crystalline $Ba_3NbFe_3Si_2O_{14}$. The data clearly show that above T_N there are short-range correlations between spins at the nearest-neighbor and next-nearest-neighbor Fe sites. Below T_N, a well-defined spin wave develops, which could be understood by a Heisenberg Hamiltonian based on a distorted triangular magnetic structure with nearest-neighbor and next-nearest-neighbor interactions. A model is developed to describe the in-plane excitations involving inter- and intratrimer interactions which are crucial toward a complete understanding of the ordering process and bulk magnetic properties of $Ba_3NbFe_3Si_2O_{14}$.

The elastic and inelastic neutron-scattering measurements were completed at the NIST CHRNS using the disk chopper spectrometer (DCS) with wavelengths of 4.8 and 2.5 Å on an oriented $Ba_3NbFe_3Si_2O_{14}$ single-crystal sample. The scattering plane of the central bank of DCS detectors is the *ab* plane. The powder neutron-diffraction patterns were obtained using BT1.

Elastic neutron-scattering data with momentum transfers within the $(H,K,0)$ plane measured at 40 K (Fig. 2), well above T_N, clearly show that a considerable amount of diffuse scattering is superimposed on the nuclear Bragg peaks, as pointed out by the arrow in Fig. 2(b). Diffuse scattering is also present at temperatures on the order of the Weiss constant $\theta=-190$ K, as seen in the $T=200$ K data set near $Q=0$.[12] By decreasing the temperature to 1.5 K, well below T_N, the diffuse scattering disappears and new magnetic Bragg peaks emerge (Fig. 2). The diffuse scattering is centered on points within the Brillouin zone commensurate with the lattice. This is due to nearly gapless excitations (within our energy resolution) that have minima calculated in our spin-wave analysis discussed at a later point in this Brief Report.

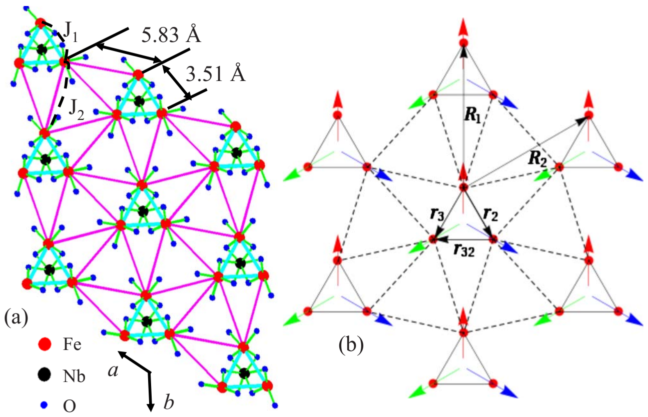

FIG. 1. (Color online) (a) The two-dimensional Fe^{3+} triangles in the *ab* plane for $Ba_3NbFe_3Si_2O_{14}$; (b) the distorted triangular magnetic lattice built by connecting the nearest-neighbor and next-nearest-neighbor interactions, which is used for the calculation described in the text. $\mathbf{R}_1$ and $\mathbf{R}_2$ are the triangular Bravais lattice basis vectors and $\mathbf{r}_2$ and $\mathbf{r}_3$ denote sublattice vectors.

As shown from the temperature dependence of the integrated intensity of the diffuse scattering obtained from powder neutron-diffraction patterns (Fig. 2), this diffuse scattering already appears at 60 K, which is well above the magnetic transition at 26 K. On cooling, the integrated diffuse scattering rises in intensity and seems to be most pronounced around 40 K. On further cooling, the scattering becomes weaker below the long-range magnetic-ordering temperature but still exists at 20 K. By 5 K, the data show no discernible sign of the diffuse scattering above background. This behavior suggests that magnetic correlations exist at much higher temperatures than the ordering temperature, which is not surprising considering the frustrated topology of the spins and the large Weiss constant $\theta = -190$ K. The maximum in the diffuse scattering intensity at 40 K is unusual though, and this can be explained by investigating the inelastic magnetic excitation spectrum.

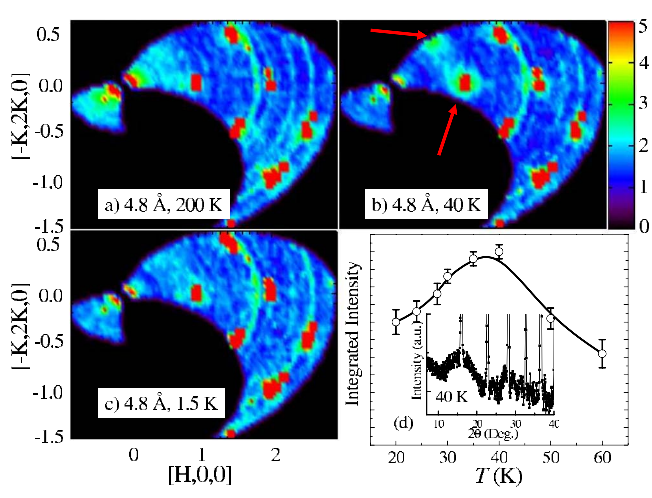

FIG. 2. (Color online) Elastic neutron scattering ($-0.1 < E < 0.1$ meV) within $(H,K,0)$ plane measured with $\lambda = 4.8$ Å at (a) $T = 200$ K, (b) $T = 40$ K, and (c) $T = 1.5$ K for $Ba_3NbFe_3Si_2O_{14}$. The diffuse scattering is noted by the red arrow in (b). The temperature dependence of the integrated intensity of the diffuse scattering from the powder neutron-diffraction data is shown in panel (d). Inset: the powder neutron-diffraction pattern at 40 K as measured on BT1. Error bars represent $\pm 1\sigma$.

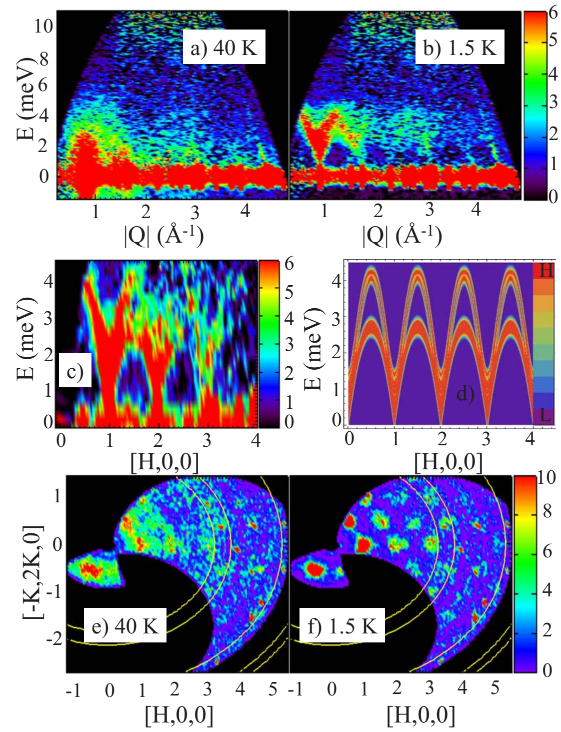

FIG. 3. (Color online) Inelastic neutron-scattering patterns measured with $\lambda = 2.5$ Å for $Ba_3NbFe_3Si_2O_{14}$. (a) and (b) Powder pattern with (a) $T = 40$ K and (b) $T = 1.5$ K. (c) Single-crystal pattern with $T = 1.5$ K by making cut of $K = [-0.1, 0.1]$. (d) The spin-wave dispersion along the $[H,0,0]$ direction within the cut $K = [-0.1, 0.1]$ for $J_1 = 0.48$ meV and $J_2 = 0.29$ meV calculated from Eq. (2) within linear spin-wave theory. (e) and (f) Single-crystal pattern within $(H,K,0)$ plane by making cut of $E = [-1.8, 2.2]$ meV with (e) $T = 40$ K and (f) $T = 1.5$ K. The yellow lines are Al powder lines from the cryostat.

As shown in Fig. 3(a), the diffuse scattering appears to extend well into the inelastic region, at least to $E = 5$ meV. With decreasing temperature, these excitations develop to a well-defined spin wave at 1.5 K, as shown from Fig. 3(b). The spin wave clearly shows a maximum of intensity around $Q = 0.85$ Å^{-1}. The periodic behavior of this spin-wave spectrum can be resolved along the $[H,0,0]$ direction by integrating $K = [-0.1, 0.1]$ as shown in Fig. 3(c). Furthermore, by integrating $E = [1.8, 2.2]$ meV as shown in Figs. 3(e) and 3(f), the spin-wave spectrum shows a well-defined hexagonal pattern in the $(H,K,0)$ plane at 1.5 K. By 40 K, the inelastic spectrum is not well defined, but there is a considerable amount of spectral weight due to spin fluctuations. The loss of elastic scattering intensity is correlated with the development of well-defined spin waves as the magnetic transition is approached from above, suggesting that there is an ordering of short-range spin clusters as the long-range spiral structure develops along the *c* axis.[11]

For the analysis of experimental results we calculate the spin-wave excitation in the long-range antiferromagnetic ordering phase within linear spin-wave theory. We consider a Heisenberg Hamiltonian,

$$\mathcal{H} = J_1 \sum_{i,\langle\alpha,\beta\rangle} \mathbf{S}_{i,\alpha}\cdot\mathbf{S}_{i,\beta} + J_2 \sum_{\langle i,j\rangle,\alpha\neq\beta} \mathbf{S}_{i,\alpha}\cdot\mathbf{S}_{j,\beta}, \quad (1)$$

with nearest intratrimer and nearest intertrimer antiferromagnetic exchange interactions J_1 and J_2, respectively, i,j denote the lattice vectors of a triangular lattices $\mathbf{R}_i$ and $\mathbf{R}_j$ with a lattice basis $\mathbf{R}_1=(0,c)$ and $\mathbf{R}_2=(\sqrt{3}c/2,c/2)$, where $c=8.52$ Å is the next-nearest intertrimer distance, and $\alpha,\beta=1,2,3$ denote the sublattice vectors $\mathbf{r}_\alpha$, $\mathbf{r}_1=(0,0)$, $\mathbf{r}_2=(a/2,-\sqrt{3}a/2)$, and $\mathbf{r}_3=(-a/2,-\sqrt{3}a/2)$, where $a=3.51$ Å is the Fe^{3+} distance within the trimer. We consider Néel ordered states in which intratimer spins are oriented $2\pi/3$ apart within some plane in spin space hereafter taken to be the x-z plane. To proceed we substitute rotated spin operators $\widetilde{\mathbf{S}}$ in Eq. (2) defined as

$$\widetilde{\mathbf{S}}_{i,\alpha} = (\cos\,\theta_{i,\alpha}S^x_{i,\alpha} - \sin\,\theta_{i,\alpha}S^z_{i,\alpha}, S^y_{i,\alpha}, \cos\,\theta_{i,\alpha}S^z_{i,\alpha} + \sin\,\theta_{i,\alpha}S^x_{i,\alpha}), \quad (2)$$

where $\theta_{i,1}=0$, $\theta_{i,2}=2\pi/3$, and $\theta_{i,3}=4\pi/3$ account for the local spin orientation on each sublattice. Defining the spin fluctuations away from the $2\pi/3$ classical Néel state in terms of linearized Holstein-Primakoff (HP) bosonic operators $a_{i,\alpha}$: $\widetilde{S}^z_{i,\alpha}=S-a^\dagger_{i,\alpha}a_{i,\alpha}$, $\widetilde{S}^+_{i,\alpha}=\sqrt{2S}a_{i,\alpha}$, and $\widetilde{S}^-_{i,\alpha}=\sqrt{2S}a^\dagger_{i,\alpha}$ and keeping only quadratic terms in $1/S$ expansion, $\mathcal{H}=\mathcal{E}_0+\mathcal{H}_2+\cdots$, $\mathcal{E}_0=-(3/2)NJ_1S^2(1+2J_2/J_1)$ is energy of the classical $2\pi/3$ Néel state and

$$\mathcal{H}_2 = \frac{3J_1S}{2}\left(1+2\frac{J_2}{J_1}\right)\sum_k\left[(\alpha^\dagger_{\mathbf{k}}\alpha_{-\mathbf{k}})H_2(\mathbf{k})\begin{pmatrix}\alpha_{\mathbf{k}}\\ \alpha^\dagger_{-\mathbf{k}}\end{pmatrix}\right], \quad (3)$$

where $\alpha^\dagger_{\mathbf{k}}=(a^\dagger_{1,\mathbf{k}},a^\dagger_{2,\mathbf{k}},a^\dagger_{3,\mathbf{k}})$, is the Fourier transform of the bosonic HP operators and $H_2(\mathbf{k})$ is a 6×6 matrix of the form

$$H_2(\mathbf{k}) = \begin{pmatrix}\mathbb{I}+\Gamma & -3\Gamma\\ -3\Gamma & \mathbb{I}+\Gamma\end{pmatrix}, \quad (4)$$

where Γ is a 3×3 off-diagonal Hermitian matrix with the following upper triangular complex matrix elements:

$$\gamma_{12} = \frac{\left[e^{-i\mathbf{k}\cdot\mathbf{r}_2} + \frac{J_2}{J_1}\left(e^{-i\mathbf{k}\cdot(\mathbf{R}_1+\mathbf{r}_2)} + e^{-i\mathbf{k}\cdot(\mathbf{R}_1-\mathbf{R}_2+\mathbf{r}_2)}\right)\right]}{4\left(1+2\frac{J_2}{J_1}\right)},$$

$$\gamma_{13} = \frac{\left[e^{-i\mathbf{k}\cdot\mathbf{r}_3} + \frac{J_2}{J_1}\left(e^{-i\mathbf{k}\cdot(\mathbf{R}_2+\mathbf{r}_3)} + e^{-i\mathbf{k}\cdot(\mathbf{R}_1+\mathbf{r}_3)}\right)\right]}{4\left(1+2\frac{J_2}{J_1}\right)},$$

$$\gamma_{23} = \frac{\left[e^{-i\mathbf{k}\cdot\mathbf{r}_{32}} + \frac{J_2}{J_1}\left(e^{-i\mathbf{k}\cdot(\mathbf{R}_2+\mathbf{r}_{32})} + e^{-i\mathbf{k}\cdot(\mathbf{R}_2-\mathbf{R}_1+\mathbf{r}_{32})}\right)\right]}{4\left(1+2\frac{J_2}{J_1}\right)}, \quad (5)$$

which correctly reduces to the case of a triangular lattice for $c=\sqrt{3}a$.[15]

The Hamiltonian $\mathcal{H}_2(\mathbf{k})$ can be diagonalized by the generalized Bogoliubov transformation which for the case of bosons amounts to calculating the eigenvalues of $H_2(\mathbf{k})$ multiplied by a sympletic matrix $\mathcal{J}=\mathbb{I}_{3\times3}\otimes\sigma^3$,[16] where σ^3 is the Pauli matrix. Figure 3(d) shows a plot of the spin-wave excitation for a cut $k_ya=(-0.3,0.3)$ in the Brillouin zone for a given value of $J_1=0.48(5)$ meV and $J_2=(a/b)J_1=0.29(3)$ meV, $b=5.83$ Å (nearest intertrimer distance).[17] The spin-wave spectrum consists of three different branches of excitations which matches the experimental data of Fig. 3(c) quite well. The calculated spectrum clearly indicates the relevance of the antiferromagnetic intertrimer exchange J_2 to the long-range ordered state. The intertrimer interactions provide another route toward additional frustration in this compound similar to the case of the square lattice with nearest-neighbor antiferromagnetic and next-nearest-neighbor ferromagnetic interactions. In this case, however, the interactions are both antiferromagnetic and involving a hexagonal interconnection of spin trimers. A full calculation of the spin-wave spectrum involving out-of-plane correlations and possible spin canting due to the Dzyaloshinsky-Moriya interaction[18] [such as in the iron jarosite system $KFe_3(OH)_6(SO_4)_2$ (Ref. 19)] would involve higher energy resolution scans of a possible spin gap.

As the various experimental probes are considered, a magnetic-ordering process in $Ba_3NbFe_3Si_2O_{14}$ begins to emerge: at high temperatures, there is a short-range ordered state characterized by a broad feature in the diffuse scattering developing by 60 K. As the temperature is cooled, the diffuse scattering grows in intensity, but by 40 K the diffuse scattering intensity saturates and begins to decrease, indicative of the development of gapped excitations outside of the elastic energy resolution. Both spin chiralities are likely present at high temperatures above T_N in the spin clusters as there is no physical reason for one preference over the other until symmetry is broken at the magnetic transition.[20] The ordering process must involve the reorganization of spin clusters of different chiralities into a uniform chirality, as there is only one chirality noted within the magnetic structure.[11,21] Fe^{3+} spins on a triangle have only two possible chiral states, which means that this order takes on a discrete or Ising character. By 40 K, long-range correlations develop and must involve the intertrimer interactions to establish one chirality (as noted with the spin-wave calculations). Interestingly, within the ordered phase, short-range correlations of spins still exist down to at least 20 K. The coexistence of short-range ordered spin clusters within the antiferromagnetically ordered state has been observed for other frustrated magnetic systems,[5,22–24] and in this case it is likely to arise from orphan spin clusters of opposing chirality that remains within the lattice. Finally at 1.5 K, the long-range magnetic-ordering structure with one chirality is completed and a spin-wave spectrum is well defined. In this process, both intratrimer and intertrimer interactions play key roles in the establishment of the unique magnetic structure.

Recently we reported a rise of electric polarization along the c axis around T_N in $Ba_3NbFe_3Si_2O_{14}$, suggesting that the sample is a multiferroic.[12] The origin of this multiferroicity is still a matter of debate. Data reported here suggest that the development of the multiferroicity is a process that first involves short-range-correlated spins over triangular units with longer-ranged correlations developing by $T=40$ K, followed by a transition to a partially ordered state at T_N characterized by the organization of the vortices with a chiral pattern coexisting with uncorrelated left over orphan triangular units. Other thermodynamic measurements show a signature of this process at 40 K, appearing as broad features within the heat-capacity and thermal-conductivity measurements of crystals.[12] The scattering of long-range excitations (such as phonons and magnons) from these structures is a natural explanation for these features.

In summary, the magnetic-ordering process in $Ba_3NbFe_3Si_2O_{14}$ has been characterized by elastic and inelastic neutron scattering experiments. Both experimental data and theoretical calculations show that intratrimer and intertrimer spin exchanges must be both considered for this process. The development of a single chirality is important for the establishment of the multiferroic properties of this compound, which is now known to be a complicated process involving the systematic ordering of vortices as seen via neutron scattering.

This work utilized facilities supported in part by the NSF through the Cooperative Agreements No. DMR-0654118, DMR-0454672, and DMR-0944772.

*zhou@magnet.fsu.edu

[1] R. Coldea, D. A. Tennant, and Z. Tylczynski, Phys. Rev. B **68**, 134424 (2003).

[2] C. Stock, L. C. Chapon, O. Adamopoulos, A. Lappas, M. Giot, J. W. Taylor, M. A. Green, C. M. Brown, and P. G. Radaelli, Phys. Rev. Lett. **103**, 077202 (2009).

[3] Y. Shimizu, K. Miyagawa, K. Kanoda, M. Maesato, and G. Saito, Phys. Rev. Lett. **91**, 107001 (2003).

[4] S. Nakatsuji, Y. Nambu, H. Tonomura, O. Sakai, S. Jonas, C. Broholm, H. Tsunetsugu, Y. M. Qiu, and Y. Maeno, Science **309**, 1697 (2005).

[5] J. Park, J. G. Park, G. S. Jeon, H. Y. Choi, C. Lee, W. Jo, R. Bewley, K. A. McEwen, and T. G. Perring, Phys. Rev. B **68**, 104426 (2003).

[6] M. Kenzelmann, G. Lawes, A. B. Harris, G. Gasparovic, C. Broholm, A. P. Ramirez, G. A. Jorge, M. Jaime, S. Park, Q. Huang, A. Y. Shapiro, and L. A. Demianets, Phys. Rev. Lett. **98**, 267205 (2007).

[7] C. Broholm, G. Aeppli, G. P. Espinosa, and A. S. Cooper, Phys. Rev. Lett. **65**, 3173 (1990).

[8] J. S. Helton, K. Matan, M. P. Shores, E. A. Nytko, B. M. Bartlett, Y. Yoshida, Y. Takano, A. Suslov, Y. Qiu, J. H. Chung, D. G. Nocera, and Y. S. Lee, Phys. Rev. Lett. **98**, 107204 (2007).

[9] J. D. Grohol, K. Matan, J. H. Cho, S. H. Lee, J. W. Lynn, D. G. Nocera, and Y. S. Lee, Nature Mater. **4**, 323 (2005).

[10] Y. Qiu, C. Broholm, S. Ishiwata, M. Azuma, M. Takano, R. Bewley, and W. J. L. Buyers, Phys. Rev. B **71**, 214439 (2005).

[11] K. Marty, V. Simonet, E. Ressouche, R. Ballou, P. Lejay, and P. Bordet, Phys. Rev. Lett. **101**, 247201 (2008).

[12] H. D. Zhou, L. L. Lumata, P. L. Kuhns, A. P. Reyes, E. S. Choi, N. S. Dalal, J. Lu, Y. J. Jo, L. Balicas, J. S. Brooks, and C. R. Wiebe, Chem. Mater. **21**, 156 (2009).

[13] J. S. Gardner, S. R. Dunsiger, B. D. Gaulin, M. J. P. Gingras, J. E. Greedan, R. F. Kiefl, M. D. Lumsden, W. A. MacFarlane, N. P. Raju, J. E. Sonier, I. Swainson, and Z. Tun, Phys. Rev. Lett. **82**, 1012 (1999).

[14] H. D. Zhou, C. R. Wiebe, A. Harter, N. S. Dalal, and J. S. Gardner, J. Phys.: Condens. Matter **20**, 325201 (2008).

[15] T. Jolicoeur and J. C. Le Guillou, Phys. Rev. B **40**, 2727(R) (1989).

[16] U. Zulicke, Ph.D. thesis, Indiana University, 1998.

[17] The error bars here are estimated based on full width at half maximum of the maxima in the first Brillouin zone of the dispersion curve.

[18] T. Moriya, Phys. Rev. **120**, 91 (1960).

[19] K. Matan, D. Grohol, D. G. Nocera, T. Yildirim, A. B. Harris, S. H. Lee, S. E. Nagler, and Y. S. Lee, Phys. Rev. Lett. **96**, 247201 (2006).

[20] While it is tempting to associate the $q=0$ correlations noted in our data to a uniform chirality of the clusters, polarized neutron-scattering measurements are needed to establish this.

[21] K. Marty, P. Bordet, V. Simonet, M. Loire, R. Ballou, C. Darie, J. Kljun, P. Bonville, O. Isnard, P. Lejay, B. Zawilski, and C. Simon, Phys. Rev. B **81**, 054416 (2010).

[22] O. A. Petrenko, D. M. Paul, C. Ritter, T. Zeiske, and M. Yethiraj, Physica B **266**, 41 (1999).

[23] J. R. Stewart, G. Ehlers, A. S. Wills, S. T. Bramwell, and J. S. Gardner, J. Phys.: Condens. Matter **16**, L321 (2004).

[24] I. Mirebeau, A. Apetrei, J. Rodriguez-Carvajal, P. Bonville, A. Forget, D. Colson, V. Glazkov, J. P. Sanchez, O. Isnard, and E. Suard, Phys. Rev. Lett. **94**, 246402 (2005).